Published OnlineFirst July 7, 2017; DOI: 10.1158/0008-5472.CAN-16-3127

Therapeutics, Targets, and Chemical Biology

Cancer Research

Resistance to the Antibody–Drug Conjugate T-DM1 Is Based in a Reduction in Lysosomal Proteolytic Activity

Carla Ríos-Luci[1], Sara García-Alonso[1], Elena Díaz-Rodríguez[1], Mercedes Nadal-Serrano[2], Joaquín Arribas[2,3,4,5], Alberto Ocaña[6], and Atanasio Pandiella[1,3]

Abstract

Trastuzumab-emtansine (T-DM1) is an antibody–drug conjugate (ADC) that was approved recently to treat HER2$^+$ breast cancers. Despite its impressive clinical efficacy in many patients, intrinsic and acquired resistance to T-DM1 has emerged as a challenge. To identify mechanisms of T-DM1 resistance, we isolated several resistant HER2$^+$ clones exhibiting stable drug refractoriness *in vitro* and *in vivo*. Genomic comparisons showed substantial differences among three of the isolated clones, indicating several potential mechanisms of resistance to T-DM1. However, we observed no differences in HER2 levels and signaling among the resistant models and parental HER2$^+$ cells. Bioinformatics studies suggested that intracellular trafficking of T-DM1 could underlie resistance to T-DM1, and systematic analysis of the path followed by T-DM1 showed that the early steps in the internalization of the drug were unaltered. However, in some of the resistant clones, T-DM1 accumulated in lysosomes. In these clones, lysosomal pH was increased and the proteolytic activity of these organelles was deranged. These results were confirmed in T-DM1–resistant cells from patient-derived HER2$^+$ samples. We postulate that resistance to T-DM1 occurs through multiple mechanisms, one of which is impaired lysosomal proteolytic activity. Because other ADC may use the same internalization-degradation pathway to deliver active payloads, strategies aimed at restoring lysosomal functionality might overcome resistance to ADC-based therapies and improve their effectiveness. *Cancer Res; 77(17); 4639–51. ©2017 AACR.*

Introduction

Increased levels of the transmembrane tyrosine kinase HER2 are present in 20% of breast tumors and are associated with poor patient outcome (1). Those findings, together with preclinical studies that linked HER2 overexpression to a tumorogenic phenotype (2), led to the development of agents directed to HER2 (3, 4). Two types of agents have reached the oncology clinic (4, 5). On the one hand, humanized monoclonal antibodies, such as trastuzumab (6) or pertuzumab (7), that bind to the extracellular domain of HER2, preventing HER2 signaling and also triggering immune-mediated responses (8). On the other hand, the small molecule kinase inhibitor lapatinib acts by competitively displacing ATP from its binding pocket in the intracellular region of HER2, neutralizing the kinase activity of HER2 and ultimately provoking cell-cycle arrest and apoptosis (9).

In addition to the potential oncogenic role of HER2, its overexpression on the membrane of tumor cells opened the possibility of using it as a docking site to preferentially deliver cytotoxic agents to tumor cells (10). To fight HER2 tumors, such a composite molecule has been created using trastuzumab as the backbone to which the anti-microtubular maytansinoid drug emtansine (DM1) has been linked (11). The conjugate termed trastuzumab-emtansine (T-DM1) is stable in the bloodstream and, upon interaction with cell surface HER2, is internalized and brought to intracellular compartments, where it is degraded or recycled to the cell surface. The process of degradation of T-DM1 appears critical for its antitumoral activity. In the lysosomes, acidic proteases progressively fragment the antibody part of T-DM1 releasing the active payload product Lys-MCC-DM1, which is then transported to the cytosol where it can act on tubulin (12). The targeted cells are then arrested in mitosis, which leads to cell death by mitotic catastrophe (13, 14).

T-DM1 reached the market in 2013 for the therapy of patients with HER2$^+$ metastatic breast cancer that progressed to the combination of trastuzumab and a taxane (15). Although the clinical results with T-DM1 are impressive, some patients do not respond to the drug or relapse (16, 17). In this study, we have explored the mechanism(s) of resistance to T-DM1. Genomic as well as functional studies demonstrated the presence of several mechanisms of resistance to the drug. One of them, uncovered by systematic analysis of the path followed by the drug, was linked to altered lysosomal function.

[1]Instituto de Biología Molecular y Celular del Cáncer, CSIC, Salamanca, Spain. [2]Vall d'Hebron Institut d'Oncologia (VHIO), Barcelona, Spain. [3]CIBERONC, Madrid, Spain. [4]Departamento de Bioquímica y Biología Molecular, UAB, Barcelona, Spain. [5]Institució Catalana de Recerca i Estudis Avançats (ICREA), Barcelona, Spain. [6]Unidad de Investigación Traslacional Hospital Universitario de Albacete, Albacete, Spain.

Note: Supplementary data for this article are available at Cancer Research Online (http://cancerres.aacrjournals.org/).

C. Ríos-Luci and S. García-Alonso contributed equally to this article.

Corresponding Author: Atanasio Pandiella, CSIC-University of Salamanca, Campus Miguel de Unamuno s/n, Salamanca, Salamanca 37007, Spain. Phone: 34-923-294815; Fax: 34-923-294743; E-mail: atanasio@usal.es

doi: 10.1158/0008-5472.CAN-16-3127

Published OnlineFirst July 7, 2017; DOI: 10.1158/0008-5472.CAN-16-3127

Materials and Methods

Cell culture and generation of resistant models

BT474 cell line was obtained from the ATCC (Lot number: 59538606, purchased in 2012) and cultured as recommended. Authenticity of the cells was regularly tested by short tandem repeat (STR). T-DM1 resistant clones were derived from parental cells by prolonged exposure to T-DM1 following an initial dose-response study of T-DM1 (0.1 nmol/L–100 nmol/L) over 5 days. Resistant BT474 T-DM1R cell lines were obtained by single-cell cloning and continuously cultured in the presence of 5 nmol/L T-DM1 for 3 months. Clones were routinely tested for resistance.

Cell proliferation, cell cycle and apoptosis analysis, and lentiviral knockdown of HER2

Cell proliferation was assessed by MTT metabolization, cell counting, or crystal violet as described (18, 19). Cell cycle analysis was performed as previously described (14). To determine the mitotic index, cells were seeded at low density, treated and stained with DAPI. Coverslips were observed in an Axiophot 2 Zeiss microscope with the 40× objective. For each condition, at least 1,500 cells were counted. Those in which chromosomes were condensed were considered mitotic cells. The number of apoptotic cells was determined according to the protocol accompanying the FITC Annexin V Apoptosis Detection Kit I (BD Biosciences). Cells were acquired using an Accuri C6 Flow Cytometer (BD Biosciences). Typically, 50,000 events were collected and analyzed using the C6 software. Knockdown of HER2 was performed by infection with lentiviral particles as described (14, 20).

Microarray analysis of mRNA

The procedure for the microarray experiments was as previously published (21). The enrichment analysis was performed using Enrichr software (22, 23). Microarray data were obtained from three independent replicates, and are available through the GEO repository database (GSE100192).

Measurement of T-DM1 levels on the cell surface

Cells were treated with 10 nmol/L T-DM1 for 30 minutes at room temperature. Then, cells were washed and incubated with Cy3-conjugated anti-human antibody. T-DM1 mean fluorescence levels were measured by using a BD Accuri C6 flow cytometer and the C6 software.

For cell surface immunoprecipitation, cells were washed twice with Krebs-Ringer-HEPES buffer [KRH, (24)] and incubated with 10 nmol/L T-DM1 in the same buffer for 2 hours at 4°C. Monolayers were washed twice with PBS and lysed. Cell debris was removed by centrifugation and supernatants incubated for 30 minutes with protein A-Sepharose. Immunocomplexes were then washed and loaded into SDS-PAGE and detected with the anti-human-HRP secondary antibody.

Western blotting and phospho-kinase array

The preparation of cell lysates and Western blotting procedures have been described (24–26). For the antibody arrays, 750 μg of BT474 parental and resistant clones cell lysates were hybridized to Human Phospho-Kinase Array Kit (R&D Systems; ref. 27).

Biotin labeling and internalization of T-DM1

T-DM1 was biotinylated with succinimidyl-2-(biotinamido) ethyl-1,3-dithiopropionate (EZ-Link NHS-SS-Biotin, Thermo Scientific) according to the manufacturer's instructions. Briefly, 2 mg T-DM1 was incubated with a 20-fold molar excess of a 10 mmol/L NHS-SS-Biotin solution in DMSO. The nonreacted NHS-SS-Biotin was quenched with 50 mmol/L of NH_4Cl.

Cells were pulsed with 10 nmol/L biotin-labeled T-DM1 for 30 minutes at 4°C, then washed to remove any unbound biotin-T-DM1 and chased for the indicated times at 37°C. Non-internalized biotin-labeled T-DM1 was removed by washing three times with ice-cold freshly prepared cleavage buffer (50 mmol/L glutathione, 75 mmol/L NaCl, 1 mmol/L $MgCl_2$, 0.1 mmol/L $CaCl_2$, 80 mmol/L NaOH, and 10% FBS. pH = 8.6). Cells were then washed twice with PBS and lysed in ice-cold lysis buffer (150 mmol/L NaCl, 1 mmol/L EDTA, 10% glycerol, 40 mmol/L HEPES pH 7.4, 1% Nonidet P-40, and phosphatase and protease inhibitors). Biotin-labeled T-DM1 was immunoprecipitated with Streptavidin-Sepharose High Performance (GE Healthcare), for at least 2 hours at 4°C. Immunocomplexes were recovered, washed, and resolved by SDS-PAGE and standard Western blotting.

Immunofluorescence and phase contrast microscopy

T-DM1 detection is detailed in Supplementary Materials and Methods. Acidic organelle staining was followed with 100 nmol/L LysoTracker Red DND-99 (Molecular Probes), which was added 30 minutes before fixing. Phase contrast images were obtained using conventional photomicroscopy.

pH analyses of acidic intracellular compartments and cathepsin B activity assay

To evaluate lysosomal pH, T-DM1 was labeled with pHrodo Red Microscale Labeling Kit (Thermo Scientific), according to the manufacturer's instructions Fluorescence emission was monitored by regular epifluorescence microscopy, using a Nikon Eclipse Ti-S microscopy (Nikon). Cells were collected and acquired using an Accuri C6 Flow Cytometer to quantify FL2H-positive cells. Cathepsin B enzymatic activity in live cells was measured using Magic Red Cathepsin B Detection Kit (Immunochemistry Technologies), following the manufacturer's instructions.

Xenograft studies

Female BALB/c *nu/nu* mice (7 weeks old) were purchased from Charles River Laboratories and kept in pathogen free housing in the Animal Facility following legal guidelines. Experiments received approval from the National Research Council Bioethics Subcommittee. A total of 5×10^6 cells resuspended in 50 μL of DMEM and 50 μL of Matrigel (BD Biosciences) were injected orthotopically into the caudal mammary gland of each mouse. When tumors reached a volume of 700 mm^3, animals ($n = 10$ per cell line) were randomized to two groups with similar mean tumor volumes that were intravenously treated with vehicle alone or T-DM1 (3 mg/kg). Tumor diameters were measured as described (27). Mice were sacrificed on day 21 or when the tumor volume approached 2,000 mm^3. Tumor samples were then collected and immediately frozen in liquid nitrogen. T-DM1 was analyzed by immunoprecipitation with protein A-Sepharose, and Western blotting with HRP-conjugated anti-human secondary antibody.

Published OnlineFirst July 7, 2017; DOI: 10.1158/0008-5472.CAN-16-3127

Patient data and patient-derived xenograft-derived–resistant models

PDX118 model was established from a cutaneous metastasis biopsy obtained at Vall d'Hebron Institute of Oncology (VHIO). The breast tumor sample used in this study was from a surgical resection at Vall d'Hebron University Hospital and was obtained following the Declaration of Helsinki on ethical principles for medical research involving human subjects. Written informed consent for the performance of tumor molecular studies was obtained from the patient who provided tissue. NOD.CB17-Prkdc^{scid}/J (NOD/SCID) mice used to establish the patient-derived xenograft (PDX) were maintained and treated in accordance with institutional guidelines of Vall d'Hebron University Hospital Care and Use Committee.

The cell cultures derived from PDX118 were established and characterized at Vall d'Hebron Institute of Oncology (VHIO) as previously described (19). The continuous treatment of these cells with increasing concentrations of T-DM1 led to the appearance of two independent resistant cells called TD44 and TD55.

Statistical analyses

For microarray analyses, differentially expressed genes (DEG) were selected with a fold-change ≥ 2 and ANOVA P value ≤ 0.05. Comparisons of continuous variables between two groups were performed using a two-sided Student t test. Differences were considered to be statistically significant when P values were less than 0.05. Statistical data are presented as the mean $\pm$ SD. All data were analyzed using the statistical software SPSS 21.0 (SPSS Inc.).

Results

Generation of T-DM1–resistant HER2$^+$ breast cancer cells

Because of their longstanding use as model for the study of HER2 biology and targeting, we selected the BT474 cell line to generate T-DM1–resistant cells. BT474 cells were treated for a total of 3 months in the presence of different concentrations of T-DM1 (Fig. 1A). Four resistant clones (C#1, C#2, C#3, and C#6) were obtained, as indicated by (i) failure of T-DM1 to provoke cell rounding (Fig. 1B) and (ii) failure of T-DM1 to affect their

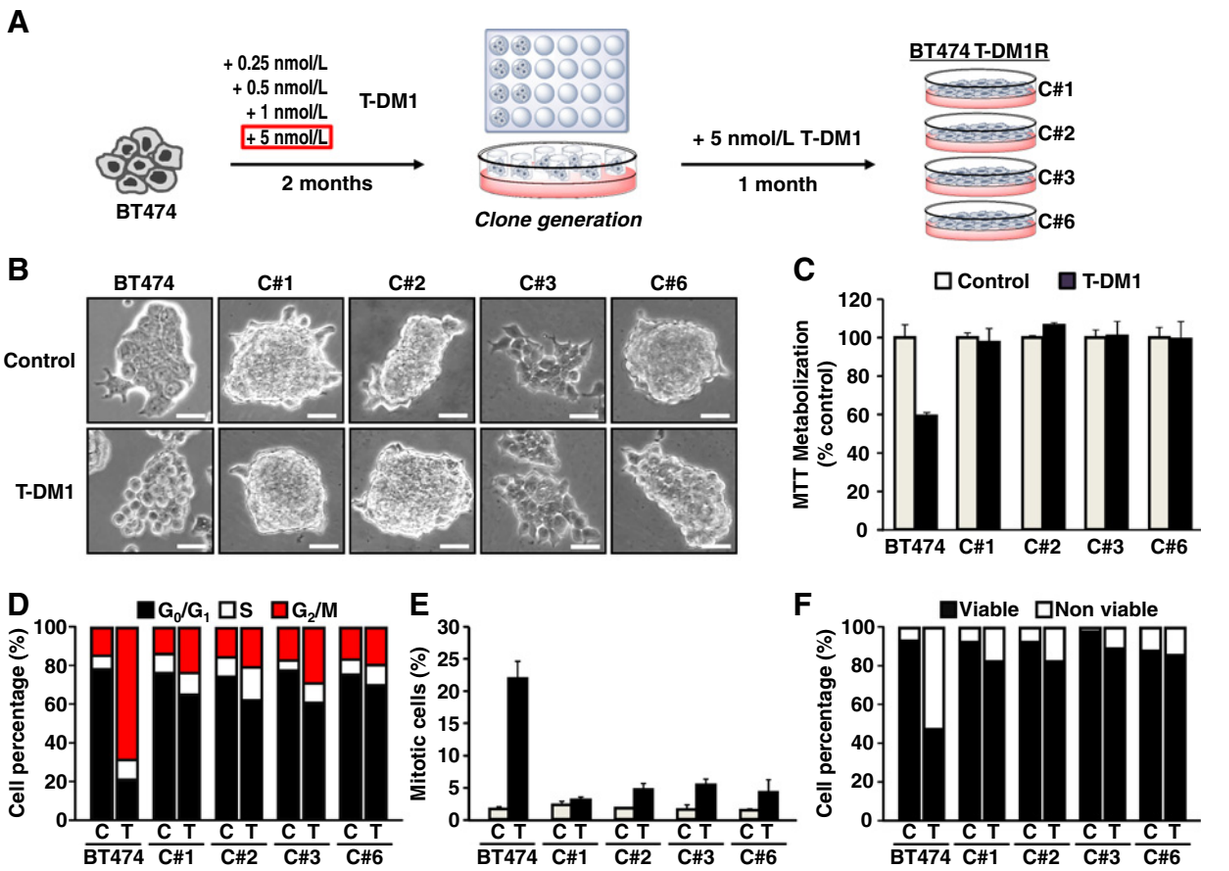

Figure 1.

Generation of T-DM1–resistant HER2$^+$ cell lines. **A,** Schematic representation of T-DM1–resistant cell lines generation. BT474 cells were treated for 2 months with the indicated T-DM1 concentrations, and resistant cells upon persistent exposure to 5 nmol/L concentrations of T-DM1 subcloned and maintained for an additional month in 5 nmol/L T-DM1. **B,** Morphologic changes induced by T-DM1 in parental and T-DM1–resistant clones. Cells cultured in 6-well plates were treated with 5 nmol/L T-DM1 for 3 days. Phase contrast images were taken at $\times$20 magnification. Scale bar, 50 μm. **C,** Proliferation of T-DM1–resistant clones. Parental BT474 and the T-DM1–resistant clones were treated with 5 nmol/L T-DM1 for 5 days and proliferation measured by MTT metabolization was normalized to control untreated cells. **D,** Effect of T-DM1 on the cell cycle. Cells were treated with T-DM1 (5 nmol/L) and cell-cycle distribution analyzed by propidium iodide staining and FACS. **E,** T-DM1 provokes accumulation of mitotic cells in wild-type BT474 cells. All cell lines were treated, fixed, and stained with DAPI to determine mitotic cells. For each condition, at least 1,500 cells were counted. Mean $\pm$ SD from three independent experiments are represented. **F,** Effect of T-DM1 on cell death. Cells were costained with Annexin V-FITC and propidium iodide, followed by FACS analysis. Viable and nonviable cells are represented. C, control; T, 5 nmol/L T-DM1 for 5 days.

Published OnlineFirst July 7, 2017; DOI: 10.1158/0008-5472.CAN-16-3127

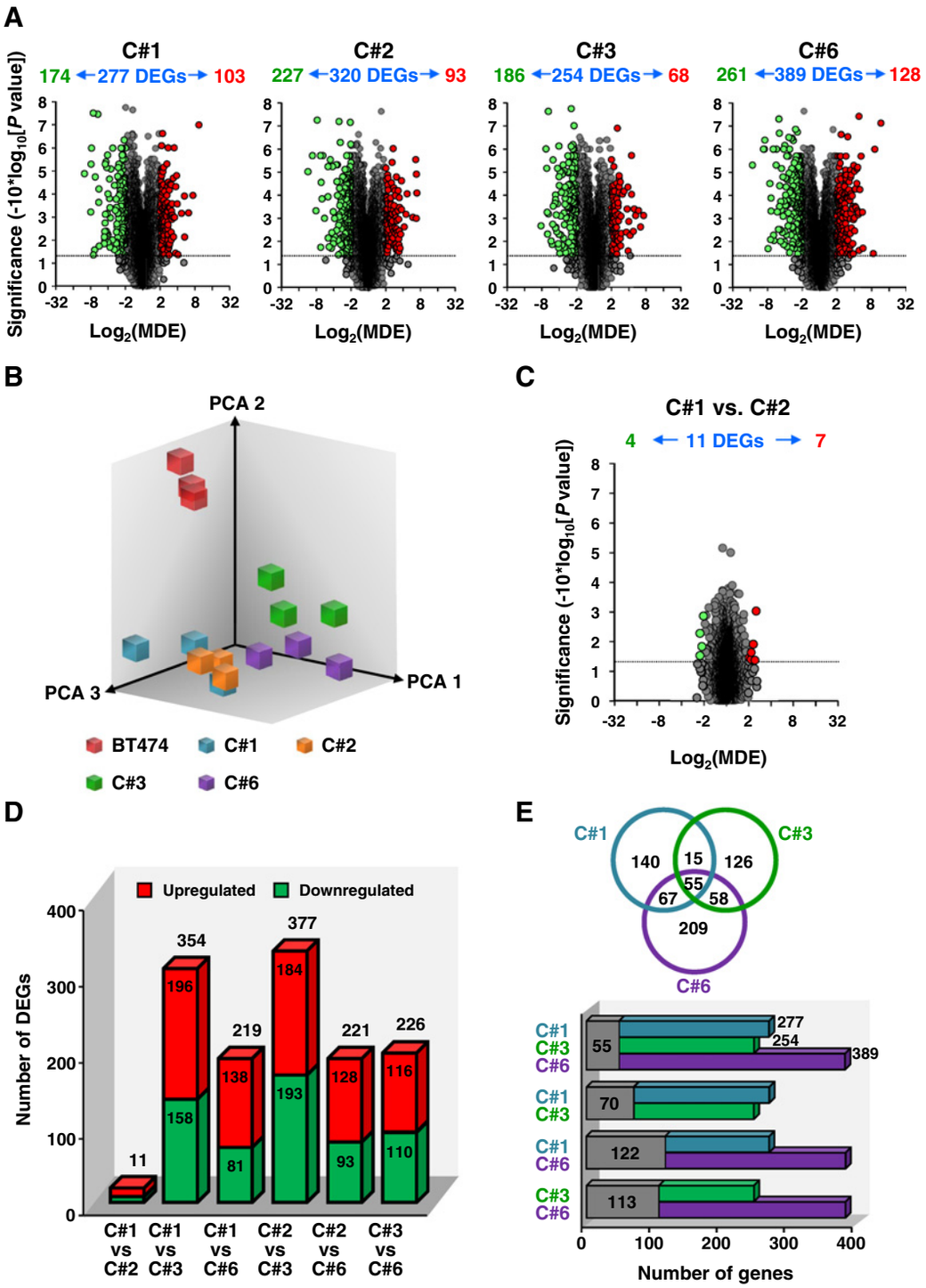

Figure 2.

Genomic characterization of T-DM1–resistant cell lines. **A,** DEGs in T-DM1–resistant clones versus the parental cell line BT474. Cut-off for DEGs was ≥2-fold change and a *P* value ≤ 0.05 and genes that meet both criteria are colored green, if downregulated, or red, if upregulated; genes filtered out are gray colored. The *y*-axis represents the significance as −10 × log of the *P* value. The *x*-axis represents the log base 2 of the mean differential expression (MDE). **B,** Principle component analysis (PCA) of variance between signal data. The graph axes represent the top three variables (PCA1, PCA2, and PCA3) that account for the majority of the variability among the samples. Replicates from each sample (same color) are labeled in the principle component analysis graph. **C,** DEGs of T-DM1–resistant clone C#1 versus C#2, analyzed as in **A**. **D,** Number of DEGs among all T-DM1–resistant cell lines. Total DEGs for each comparison are indicated above the bar. **E,** DEGs shared by T-DM1–resistant clones. Top, Venn diagram depicting the overlap of genes with modified expression levels in clones C#1, C#3, and C#6 versus the parental cell line. Bottom, colored bars denote total number of DEGs for each clone. Common gray portion of the bars represents the number of shared DEGs in clones indicated at the left.

Published OnlineFirst July 7, 2017; DOI: 10.1158/0008-5472.CAN-16-3127

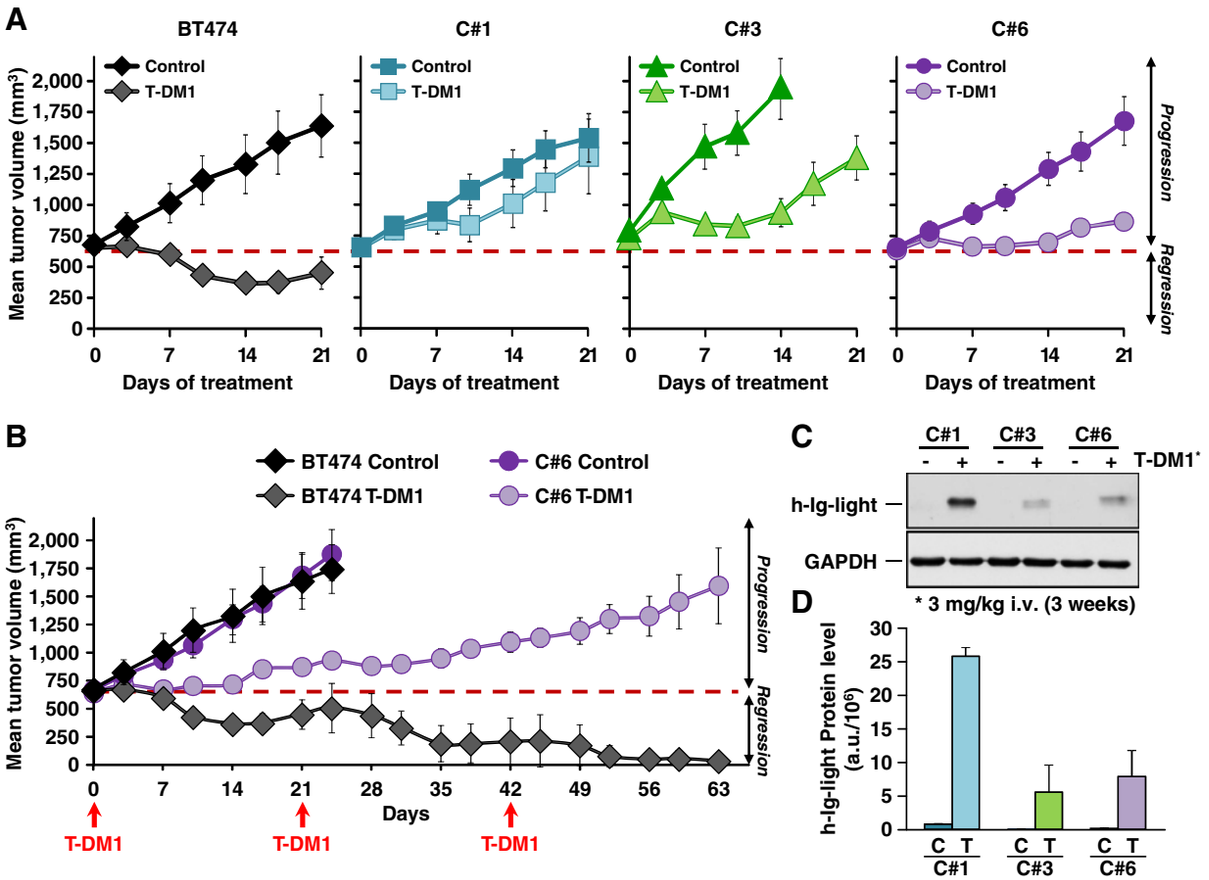

Figure 3.

In vivo effect of T-DM1. **A,** *In vivo* effect of T-DM1 on tumor growth in mice injected with wild-type and T-DM1–resistant cells. Data represent mean ± SD. Red line indicates volumes of the tumors at the time of treatment (around 700 mm^3), which was used to determine tumor progression or regression. **B,** *In vivo* effect of extended treatment with T-DM1. Animals injected with BT474 or C#6 cells were treated with T-DM1 as indicated. Tumors were measured twice a week and mean ± SD of the different groups is shown in the graph. **C,** T-DM1 accumulation in control and T-DM1–treated tumors. Three weeks after treatment with T-DM1, tumors resected from animals were analyzed for T-DM1 levels by Western blotting. GAPDH was used as loading control. **D,** Quantitation of T-DM1 levels in control and T-DM1–treated tumors. The graph represents mean ± SD of three different tumors.

proliferation (Fig. 1C). Moreover, cell-cycle profiling of the T-DM1–resistant clones showed that they were largely resistant to the effect of the drug (Fig. 1D). Quantitative analyses showed accumulation of BT474 cells in mitosis (Fig. 1E). In contrast, very few effect of the drug was observed in the clones. As expected, the mitotic arrest caused by T-DM1 provoked cell death in parental cells (Fig. 1F), probably as a consequence of mitotic catastrophe (13, 14). Such loss of viability caused by T-DM1 was marginal in T-DM1–resistant clones.

Transcriptomic and biological heterogeneity among T-DM1–resistant cells

Microarray analyses were performed to explore potential transcriptomic differences among the distinct cell lines. Volcano plots of DEGs indicated that BT474 cells differed in 277, 320, 254, and 389 genes from clones C#1, C#2, C#3, and C#6, respectively (Fig. 2A). Principal component analyses (PCA) of variance among the array data demonstrated clustering of the replicates obtained from each cell line (Fig. 2B). Such clustering is indicative of homogeneity or relationship among the gene expression profiles of different samples. Substantial differences in the three dimensional (3D) representation of PCA were observed among wild-type BT474 cells and the other clones. Importantly, clones C#1 and C#2 fell in the same region of the 3D plot (Fig. 2B). Moreover, comparative gene expression profiling between those two clones showed that only 11 genes were differentially expressed (Fig. 2C). The same comparative analyses between the other clones were performed. Despite the low number of DEGs observed between clones C#1 and C#2, a much larger number of genes appeared differentially expressed when performing comparison among the rest of them (Fig. 2D). Therefore, clones C#1 and C#2 were probably constituted by identical populations of cells and, for that reason, we decided to subsequently use clone C#1 as representative of both.

Having established that clones C#1, C#3, and C#6 were different from the gene expression profiling point of view, we analyzed genes shared by them, but differentially expressed when compared with BT474 cells. We observed 55 DEGs shared by the three clones (Fig. 2E). Clones C#1 and C#3 shared 70 DEGs, while clones C#1 and C#6 shared 122, and clones C#3 and C#6 shared

Published OnlineFirst July 7, 2017; DOI: 10.1158/0008-5472.CAN-16-3127

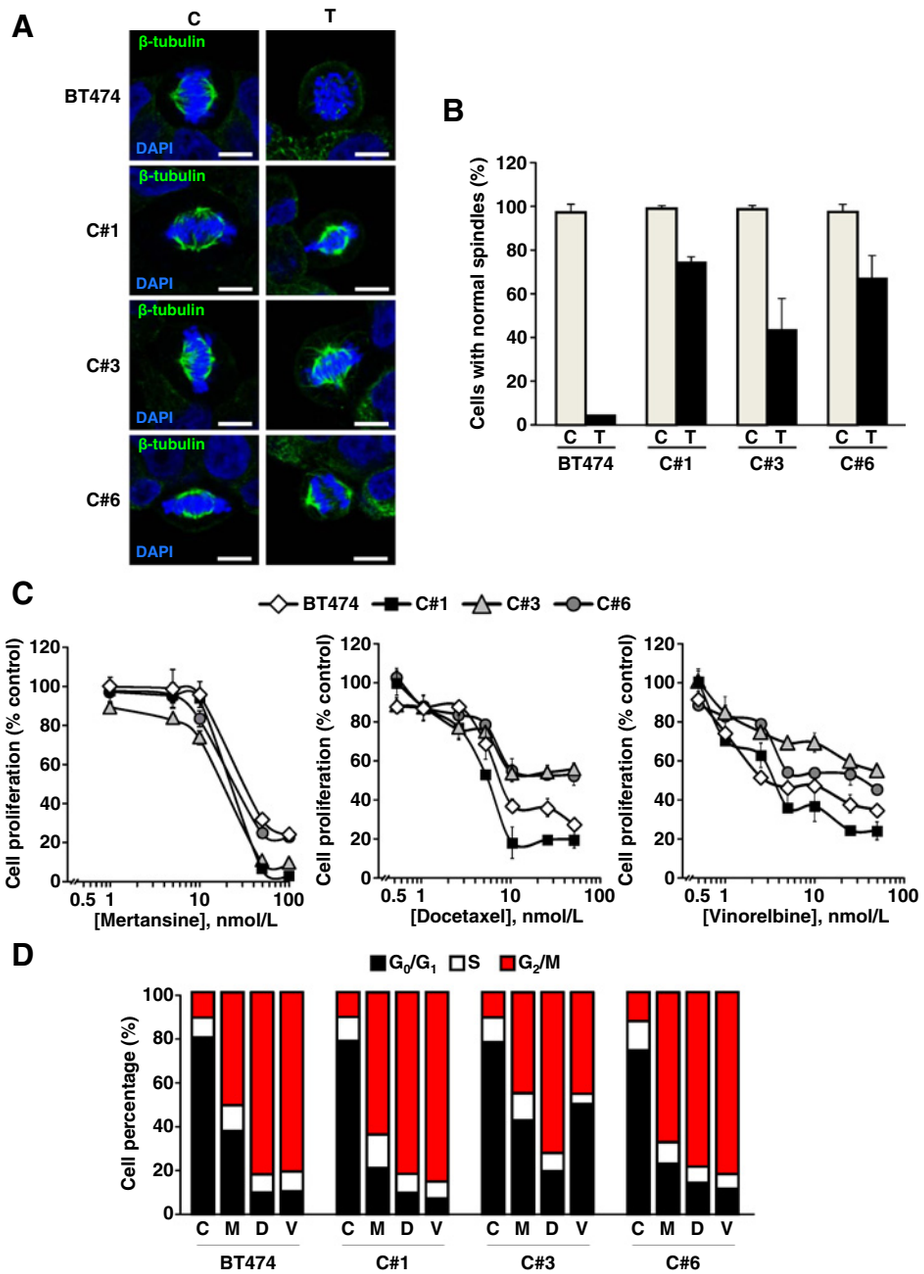

Figure 4.
Effect of T-DM1 on spindle assembly. **A,** Action of T-DM1 on mitotic spindle formation. Cell lines were treated, fixed, stained for β-tubulin (green) and DAPI (blue), and representative images taken. Scale bar, 7.5 μm. **B,** Quantitative analysis of mitotic cells with normal spindles. Bipolar spindles were evaluated in mitotic cells of the different cell lines treated or not with T-DM1. The bar graphs show the mean ± SD of two independent experiments, calculated as follows: (number of mitotic cells with normal spindles/total number of mitotic cells) ×100 (%). C, control; T, 5 nmol/L T-DM1 for 5 days. **C,** Effect of the free DM1 compound and other clinically used anti-microtubule agents on cell proliferation of wild-type and T-DM1–resistant cells. Cells were treated with increasing concentrations of mertansine, docetaxel, and vinorelbine for 3 days. Proliferation was measured by MTT metabolization and normalized to control untreated cells. Data are represented as mean ± SD of three independent experiments. **D,** Cell-cycle effect of mertansine, docetaxel, and vinorelbine in parental and resistant cells. Cells were treated with the different drugs for 24 hours and cell-cycle distribution analyzed by propidium iodide staining and FACS. C, control; M, mertansine 25 nmol/L; D, 2.5 nmol/L docetaxel; V, 2.5 nmol/L vinorelbine.

113. Together, these results suggested that clones C#1, C#3, and C#6 were different, but shared some DEGs when compared with wild-type BT474 cells.

In vivo studies also showed differences among the resistant clones. In mice injected with BT474 cells, treatment with the drug decreased tumor volume, which was not observed in the tumors of mice injected with cells from the resistant clones (Fig. 3A). However, the growth kinetics of tumors in mice treated with T-DM1 varied among the different clones. Those derived from clone C#1 were the most resistant to the *in vivo* action of T-DM1. Tumors derived from C#3 cells initially responded to T-DM1, although no regression of the tumor masses was observed. At later time points, tumors from C#3 cells regained growth. In mice injected with C#6 cells, T-DM1 treatment initially arrested tumor growth, but as occurred with the tumors generated by the other clones, no regression of tumor masses occurred. The low growth rate of the tumors of C#6 in mice treated with T-DM1 allowed us to follow for a longer time the behavior of these tumors. Of note, extension of the treatment with T-DM1 for 9 weeks caused complete regression of the tumors in mice injected with wild-type BT474 cells (Fig. 3B). However, such treatment did not prevent progressive growth of the tumor masses created by injecting C#6 cells.

Tumors from mice injected with the resistant cells were obtained and T-DM1 levels analyzed by Western blotting. Curiously, tumors derived from mice injected with cells from C#1 and

Published OnlineFirst July 7, 2017; DOI: 10.1158/0008-5472.CAN-16-3127

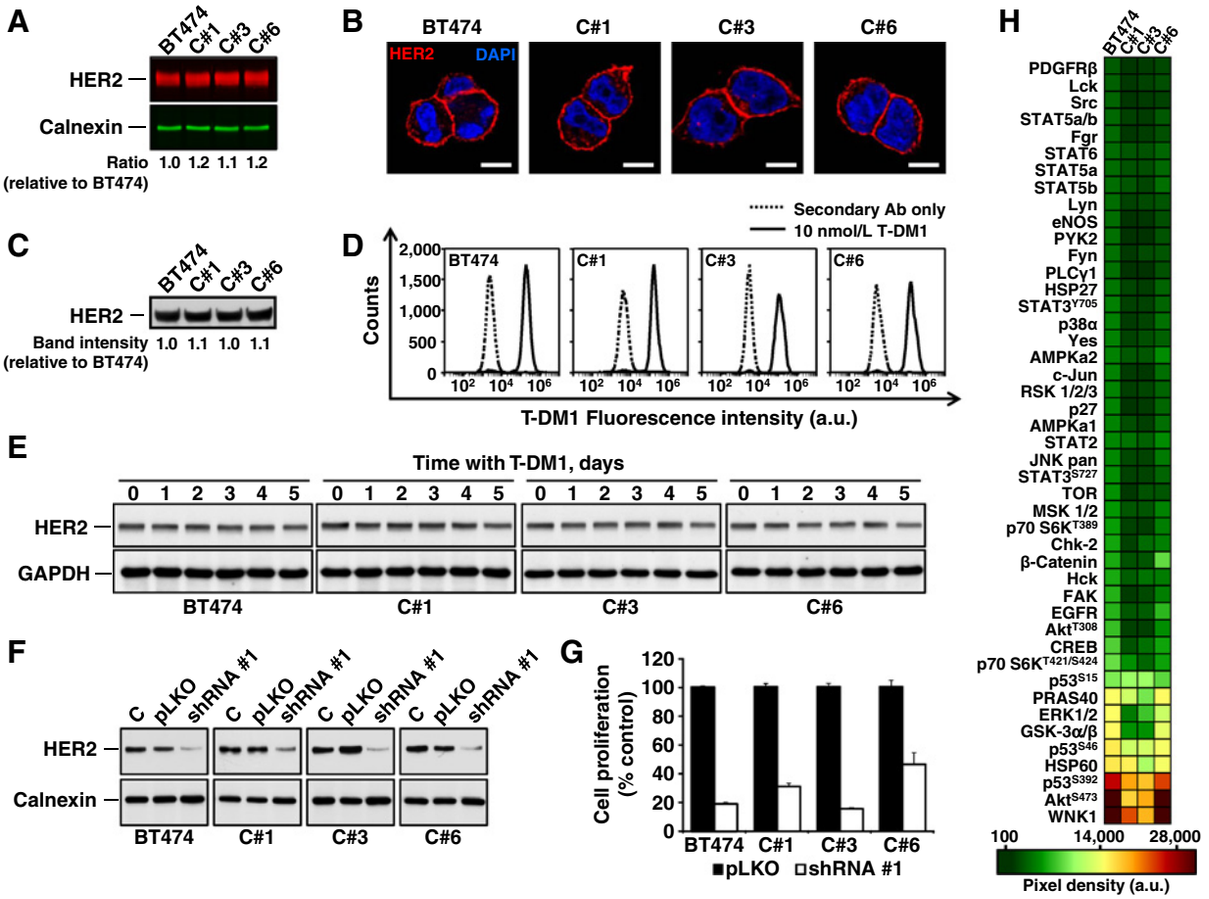

Figure 5.

T-DM1–resistant cell lines maintain HER2 levels and remain addicted to HER2. Total HER2 levels in parental and resistant cell lines analyzed by quantitative Western blotting (**A**) or by immunofluorescence (**B**). For the latter, cells were fixed and stained for HER2 (red), using trastuzumab as primary antibody, and DNA (blue). Scale bar, 7,5 μm. **C** and **D,** Cell-surface HER2 levels in parental and resistant cell lines. HER2 level was quantitatively analyzed by surface immunoprecipitation (**C**) or by flow cytometry (**D**), using T-DM1 as primary antibody in both cases. **E,** Time-course of T-DM1 effect on HER2 level. Cell lines were treated with 5 nmol/L T-DM1 for the indicated times and lysates analyzed by Western blotting with the anti-HER2 antibody. The expression of GAPDH was used as loading control. **F,** Knockdown of HER2 in BT474- and T-DM1–resistant clones. Extracts of different short hairpin (sh)-transduced cell lines were analyzed by Western blotting, with the anti-HER2 antibody (top) or the anti-calnexin antibody (bottom) used as loading control. **G,** Effect of HER2 knockdown on cell proliferation. Cells were counted after 3 days and results plotted as mean ±SD of triplicates normalized to the proliferation of sh-control transduced cells. **H,** Colorgram of the phosphorylation level of signaling proteins in parental and resistant cell lines. Each square depicts the mean of duplicate samples. Color scale represents the pixel intensity obtained from the antibody array in arbitrary units (a.u.).

treated with T-DM1 accumulated the drug to a higher extent than those derived from C#3 and C#6 cells (Fig. 3C and D).

Mitotic spindle formation in T-DM1–resistant cells

The mode of action of T-DM1 includes inhibition of microtubule polymerization during mitosis (16). T-DM1 affected the formation of normal mitotic spindles in BT474 cells, while the resistant clones were much less affected (Fig. 4A and B). As DM1 binds tubulin, altered or mutant tubulins might constitute a mechanism of resistance to T-DM1 (28). Tubulin β1 sequencing failed to show any mutations in BT474 or the resistant clones.

Cell proliferation experiments indicated that the sensitivity of the different clones to the free DM1 compound (mertansine) and other anti-microtubular agents used in the clinic, such as vinorelbine or docetaxel, was preserved (Fig. 4C). However, and in line with the different behavior of the distinct clones observed when analyzing other biological properties, differences in the anti-proliferative potency of vinorelbine or docetaxel were observed among the different clones. Cell-cycle analyses demonstrated that these agents provoked G_2–M arrest in the resistant clones as well as in wild-type BT474 cells (Fig. 4D). The above data suggested that tubulin functionality was unaltered in these clones.

T-DM1–resistant HER2$^+$ breast cancer cells remain addicted to HER2

One of the described mechanisms of resistance to anti-HER2 therapies is the loss of HER2, or the presence of truncated forms of the protein lacking the ectodomain (29, 30). As shown in Fig. 5A, no major differences among the levels of total HER2 present in the different clones and BT474 cells were observed. Moreover, immunofluorescence studies using trastuzumab to

Published OnlineFirst July 7, 2017; DOI: 10.1158/0008-5472.CAN-16-3127

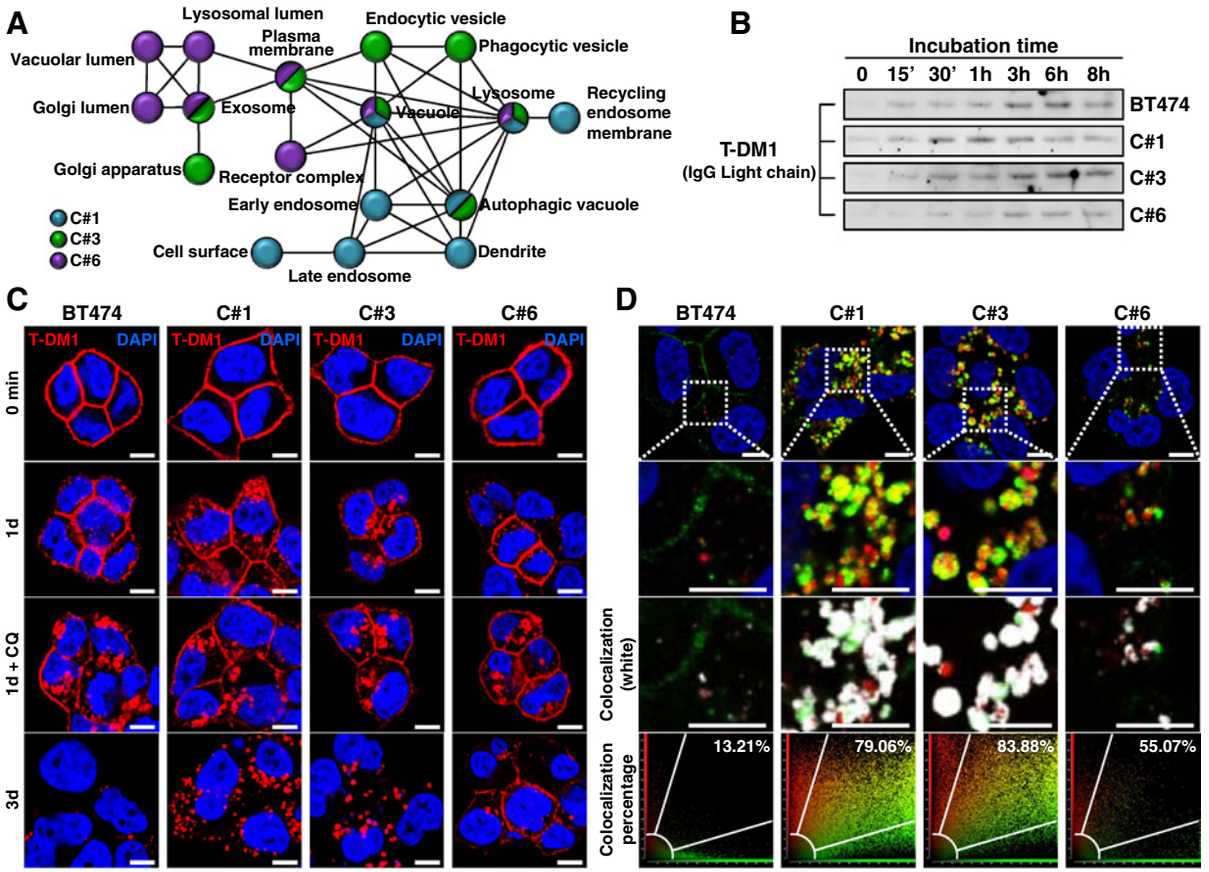

Figure 6.

Internalization of T-DM1 in parental and resistant cell lines. **A,** Microarray enrichment analysis for cellular components performed using Enrichr software. DEGs fitting the cut-off ($\geq$2-fold change and *P* value $\leq$ 0.05) in the resistant clones were classified using GO "cellular components." The network depicts the GO terms enriched in the clones. **B,** Time course of T-DM1 internalization. Cell lines were pulsed with 10 nmol/L Biotin/S-S/T-DM1 for 30 minutes at 4°C and chased at 37°C for the indicated times. Subsequently, surface accessible biotin was cleaved, cells were lysed, extracts precipitated with streptavidin-sepharose, and T-DM1 amount analyzed by Western blotting using anti–human-HRP. **C,** T-DM1 staining in the different cell lines. Cells were seeded on coverslips, pulsed with 10 nmol/L T-DM1 for 15 minutes at 37°C, and chased for the indicated times. Scale bar, 7.5 μm. CQ, chloroquine (50 μmol/L). **D,** Colocalization of T-DM1 with the acidic vesicle indicator Lysotracker. Cells were pulsed with 10 nmol/L T-DM1 for 15 minutes at 37°C, chased for 3 days, and costained with Anti-Human-Dylight 488 (T-DM1; green) and the acidic vesicle indicator LysoTracker red. Boxed areas define higher magnifications (second row). Scale bar, 7.5 μm. Colocalization between T-DM1 and LysoTracker is shown in white (third row). Image-generated scatter plots of acquired images for colocalization analysis were processed by the LAS AF software (last row). Pure red and green pixels are between abscissa/ordinate and white lines; colocalizating pixels are found inside central region of the plot (between white lines). LysoTracker/T-DM1 colocalization, calculated as the ratio of the area of colocalizing signals with respect to total fluorescence area, is indicated.

label HER2 showed similar patterns of HER2 staining in BT474 cells and the T-DM1–resistant clones (Fig. 5B). The immunofluorescence experiments also suggested that HER2 was present at the cell surface of the different cells studied at similar amounts. This was verified through quantitative analyses of cell surface HER2 levels using cell-surface immunoprecipitation (Fig. 5C) or flow cytometry (Fig. 5D). These quantitative experiments were performed using T-DM1, and, therefore, served to also demonstrate that binding of the drug to cell-surface HER2 was preserved in the resistant clones. No differences were found in HER2 levels after treatment of the cell lines with T-DM1 for prolonged incubation times (Fig. 5E).

Loss of HER2 dependency has also been proposed as another mechanism of resistance to anti-HER2 therapies (31). To explore whether such mechanism may account for the T-DM1 resistance observed in the different clones, we knocked down HER2 (Fig. 5F) and analyzed the effect on cell proliferation (Fig. 5G). These experiments demonstrated the strong dependency on HER2 of the parental BT474 cells as well as the resistant clones, indicating that they remain addicted to HER2. Together, the above data indicated that HER2 levels and dependency are preserved in the T-DM1–resistant clones.

Resistance to anti-HER2 therapies may also arise through compensatory upregulation of downstream signaling pathways, particularly the PI3K route (32, 33). The status of several signaling pathways was, therefore, analyzed using antibody arrays. The capture antibodies used in these arrays allow detection of activated forms of signaling proteins, which are used as readouts of the activity of several signaling pathways, including some activated by HER2 or PI3K activation (a schematic representation of

Published OnlineFirst July 7, 2017; DOI: 10.1158/0008-5472.CAN-16-3127

these routes can be consulted online at the Kyoto Encyclopedia of Genes and Genomes-KEGG). Antibody arrays of signaling intermediates indicated that the patterns of phosphorylation of the different proteins analyzed in C#1 and C#3 cells were similar. Clone C#6 gave a pattern of phosphoproteins more similar to BT474 cells than to the C#1 and C#3 cells (Fig. 5H). These data indicate that no evident upregulation in major downstream signaling routes was present in the T-DM1–resistant clones.

Internalization of T-DM1 in resistant cells

Because the resistance to T-DM1 did not appear to rely on molecular alterations in HER2 or tubulin, the lack of action of T-DM1 in the resistant cells could be due to increased extrusion of the payload. In fact, maytansinoids have been reported to be substrates of drug transporters such as MDR1/PgP and high levels of these proteins may confer resistance to DM1 (12). Gene expression analyses of drug transporters known to act in efflux of chemotherapeutics showed no difference in their mRNA levels (Supplementary Fig. S1), including SLC46A3, a lysosomal membrane protein, which may participate in delivery of non-cleavable antibody–drug conjugate (ADC) catabolites into the cytoplasm (34).

Gene expression profiling data were also used to explore cellular components, which could be altered in T-DM1–resistant clones. To that end, we used the Enrichr web-based tool, which is an enrichment analysis software that provides summaries of functions assigned to gene lists, including a cellular component analysis (22, 23). The gene ontology cellular component networks obtained for the gene lists corresponding to clones C#1, C#3, and C#6 showed that terms related to the endocytic pathway were enriched in all the resistant clones, having some of them in common, such as lysosome or vacuole (Fig. 6A, Supplementary Table S1). These studies pointed to endosomal trafficking or lysosomal function as subcellular processes that could be responsible for the emergence of T-DM1 resistance. To measure T-DM1 internalization, the drug was labeled using a cleavable biotin compound and the translocation of biotinylated T-DM1 to intracellular compartments was analyzed. These experiments showed that biotin/S-S/T-DM1 underwent internalization in BT474 and the resistant clones (Fig. 6B).

To gain further insights into the internalization of T-DM1 in BT474 cells and the T-DM1–resistant clones, immunofluorescence analyses were performed. Fixation of cells right after a 15 minutes pulse with T-DM1 showed that T-DM1 staining was restricted to the cell surface (Fig. 6C, 0 minute). After 1 day, cell-surface staining was still appreciable; however, punctate staining was also observed, suggesting intracellular accumulation of T-DM1. This accumulation was even more evident when using chloroquine, an agent that causes entrapment of endocytosed materials (35). *In vivo* time-lapse studies confirmed redistribution of T-DM1 from the cell surface to a punctate pattern in all the cell lines (Supplementary Movie S1). Extension of the incubation times showed differences in the patterns of T-DM1 staining. After 3 days, most of the drug had disappeared from the surface of BT474 cells and few intracellular spots remained (Fig. 6C). In contrast, in clones C#1 and C#3, a substantial amount of T-DM1 remained in punctate structures. In the case of clone C#6, some T-DM1 was still detected at the cell surface. Time-lapse studies showed progressive accumulation of the drug in such punctate structures along the time course of the experiment (Supplementary Movie S2).

Deficient lysosomal function in T-DM1–resistant cells

Colocalization experiments with markers of intracellular organelles were carried out to identify the intracellular site of T-DM1 accumulation in the resistant cells. Substantial colocalization was detected between the acidic vesicle marker LysoTracker Red DND-99 and T-DM1 after 3 days of incubation (Fig. 6D). Quantitative analysis of colocalization showed LysoTracker/T-DM1 colocalization rates of 13.21%, 79.06%, 83.88%, and 55.07% in BT474, C#1, C#3, and C#6, respectively (Fig. 6D). Moreover, colocalization with the lysosomal marker LAMP-1 (Supplementary Fig. S2) was detected in C#1 and C#3 cells.

The intracellular accumulation of T-DM1 in clones C#1 and C#3 suggested that the mechanism of resistance to the drug could be linked to deficient processing of T-DM1, likely because of altered lysosomal function. Because an acidic pH is crucial for the optimal function of lysosomal proteolytic enzymes, we evaluated whether T-DM1 reached such an acidic environment within lysosomes. To this end, T-DM1 was labeled with pHrodo, a red fluorogenic dye that is almost non-fluorescent at neutral pH, but which fluoresces in acidic environments (36). Cells were incubated with 5 nmol/L pHrodo-T-DM1 for 24 hours, and fluorescent signals analyzed *in vivo* by microscopy or by FACS. In BT474 and clone C#6 cells, fluorescence accumulated intracellularly (Fig. 7A). In contrast, in cells from clones C#1 and C#3, the fluorescent signal was much weaker. Quantitative cytometric analyses of pHrodo-T-DM1 corroborated the difference in the fluorescent signal in cells from clones C#1 and C#3 with respect to wild-type BT474 cells (Fig. 7B). These experiments suggested that the pH in the compartments reached by pHrodo-T-DM1 was substantially higher in C#1 and C#3 when compared with wild-type cells.

The proteolytic activity of lysosomes was next explored using a cathepsin B activity assay as readout (37). Cathepsin B activity of C#6 was similar to that of wild-type BT474 cells (Fig. 7C). In contrast, significantly lower cathepsin B activities were observed in clones C#1 and C#3. Taken together, the above data indicated that lysosomal pH was higher in clones C#1 and C#3, and this likely resulted in impaired overall proteolytic activity, which prevented adequate cleavage of T-DM1.

As lysosomal dysfunction could affect autophagy, the latter process was evaluated by Western blotting of LC3 processing and p62 degradation. LC3-II is degraded during autophagy. However, lysosomal degradation of LC3-II can be avoided if fusion between autophagosomes and lysosomes is blocked, using compounds such as bafilomycin A1 (38). This drug is a V-ATPase inhibitor that causes an increase in lysosomal/vacuolar pH and, ultimately, inhibits autophagy (39). As shown in Supplementary Fig. S3A and S3B, bafilomycin A1 caused an increase in LC3-II levels in parental BT474 and the resistant clones. On the other hand, p62 is primarily degraded during autophagy (38). The inductor of autophagy rapamycin provoked a decrease in p62 in all the cell lines (Supplementary Fig. S3A and S3C). Together, these data suggest that the autophagy process was preserved in all the cell lines analyzed.

If lysosomal alkalization plays a role in T-DM1 resistance, it would be expected that artificial manipulation of lysosomal pH could render BT474 cells resistant to the drug. To address that bafilomycin A1 was used. Preincubation with bafilomycin A1 caused a decrease in pHrodo-T-DM1 fluorescence, indicative of lysosomal alkalization (Fig. 7D). Moreover, bafilomycin A1 diminished the anti-proliferative action of T-DM1 in BT474 cells (Fig. 7E).

Published OnlineFirst July 7, 2017; DOI: 10.1158/0008-5472.CAN-16-3127

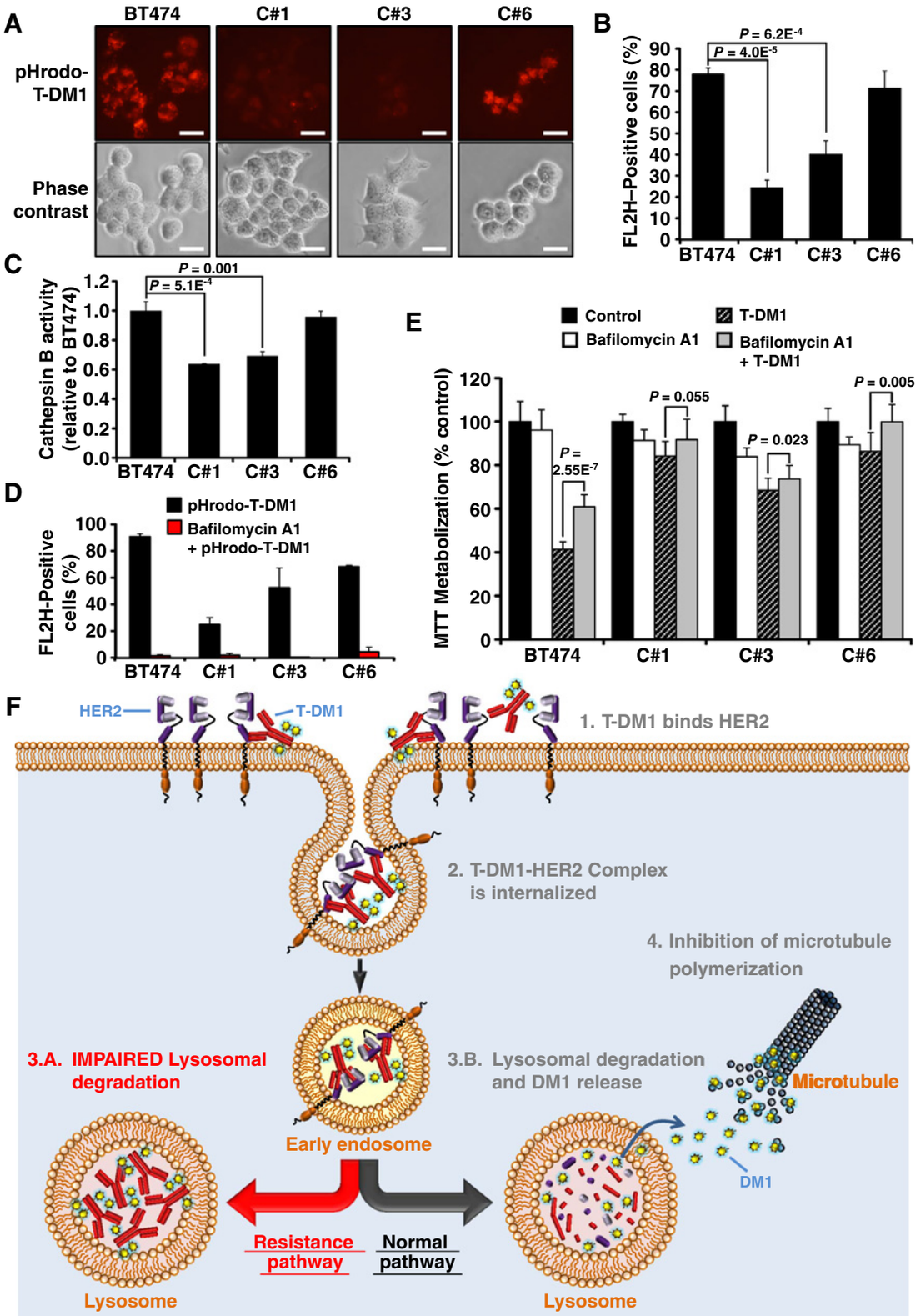

Published OnlineFirst July 7, 2017; DOI: 10.1158/0008-5472.CAN-16-3127

Finally, we explored whether the resistance mechanism described in BT474 cells also occurred in patient-derived material. To that end, we used cell cultures established from a patient-derived HER2$^+$ xenograft (PDX118; ref. 19). The initially T-DM1 sensitive cell cultures were maintained in the presence of increasing concentrations of T-DM1 for 45 days to obtain two independent cultures (TD44 and TD55, Supplementary Fig. S4A). These cells were resistant to the anti-proliferative action of T-DM1, as compared with parental cells (Supplementary Fig. S4B). Western blotting analyses confirmed the HER2$^+$ phenotype of the parental and the TD44 and TD55 cells (Supplementary Fig. S4C). Although smaller amounts of total HER2 were observed in the resistant clones, preliminary data demonstrated that resistance to T-DM1 was not due to such decrease in HER2. Staining with pHrodo-T-DM1 showed a statistically significant decrease in TD44 and TD55 cells, as compared with parental cells (Supplementary Fig. S4D). Moreover, immunofluorescence studies showed statistically significant accumulation of T-DM1 in the lysosomes of TD55 cells (Supplementary Fig. S4E and S4F).

Discussion

The development of drug resistance is a central clinical problem in oncology that, if prevented, could result in long lasting antitumoral responses. Because of this, efforts to uncover the mechanisms of resistance to anti-HER2 therapies are being made with the purpose of overcoming them.

We initiated the study herewith reported with the intention of identifying mechanisms of resistance to T-DM1, given the scarce knowledge on them and the favorable clinical responses obtained in patients treated with this drug (17). To that end, we modeled resistance using BT474 cells, and evaluated cellular processes that T-DM1 uses to carry out its effect.

Experiments aimed at exploring whether loss or truncation of HER2 were responsible for such resistance, in analogy to trastuzumab (29), failed to demonstrate an alteration in the levels of HER2 in the three T-DM1–resistant clones isolated. Furthermore, T-DM1 binding was preserved, in contrast to mechanisms of resistance to anti-HER therapies that are accompanied by loss of therapeutic antibody binding to the target (40). Moreover, knockdown experiments demonstrated oncogenic dependence on HER2 in the resistant clones, excluding the possibility that resistance to T-DM1 was caused by molecular alterations of HER2, which could cause loss of function of the protein. Finally, exploration of several signaling routes, such as PI3K, whose alteration has been linked to trastuzumab resistance (41), failed to define a clear signaling alteration in the resistant clones. So far, the data generated indicate that T-DM1 resistance in those clones is not due to a molecularly altered HER2 protein, or altered HER2-dependent signaling.

Bioinformatic analyses of gene functions pointed to the endosomal/lysosomal pathway as a route that could be involved in T-DM1 resistance. Deficient internalization of HER2 has been hypothesized as a possible mechanism of resistance to T-DM1 (42). Moreover, the already reported slow rate of internalization of HER2 (43, 44) could prime the raising of resistance to T-DM1. However, several experiments indicated that the first steps of the internalization of HER2 were preserved in the resistant clones at levels similar to those of wild-type BT474 cells. Cleavable biotinylation experiments showed that the rates of internalization of biotin-labeled T-DM1 were similar in BT474, C#1, C#3, and C#6 cells. Furthermore, *in vivo* follow-up of dye-labeled T-DM1 failed to show any defect in its early internalization steps. These results suggest that internalization was preserved in the resistant clones.

Video analyses in live cells together with more conventional immunofluorescence studies showed differences in the subcellular distribution of T-DM1, especially in long-term incubation experiments. These analyses showed that T-DM1 accumulated in intracellular compartments in C#1 and C#3 cells, but not in C#6 cells. Such accumulation of T-DM1 was also observed *in vivo*, particularly in tumors derived from C#1 cells. Studies to identify the intracellular compartment where T-DM1 was trapped in the resistant clones showed colocalization of T-DM1 with (i) the acidic compartment marker LysoTracker, (ii) antibodies recognizing LAMP-1, and (iii) a GFP-LAMP-1 fusion protein, all of them considered bona fide lysosomal markers. Assessment of lysosomal pH and cathepsin B protease activity indicated that both were altered in C#1 and C#3 cells with respect to wild-type or C#6 cells. The increase in lysosomal pH in C#1 and C#3 cells could restrict the intrinsic proteinase activities of lysosomal enzymes, impairing proteolytic cleavage of endocytosed T-DM1 (schematically illustrated in Fig. 7F). In fact, experiments in which lysosomal pH was raised in parental BT474 cells by the use of bafilomycin A1 showed that such compound decreased the antiproliferative action of T-DM1. Importantly, analyses of lysosomal pH and anti-tumoral properties of T-DM1 in resistant cells obtained from a patient-derived HER2$^+$ tumor passaged as a PDX

Figure 7.

Lysosomal function is impaired in T-DM1–resistant clones. **A,** Cells were treated with 5 nmol/L pHrodo-T-DM1 for 24 hours at 37°C and analyzed by epifluorescence microscopy. Representative microscopy images of red fluorescence and phase contrast were taken at ×40 magnification. Scale bar, 50 μm. **B,** Cells treated as in **A** were collected and analyzed by FACS. FL2H intensity indicates the percentage of red-positive cells as mean ± SD. **C,** Quantification of the proteolytic activity of lysosomal enzyme cathepsin B. Relative fluorescent was normalized to that of the parental cell line. Graph bars represent the mean ± SD of three independent experiments. **D,** Effect of bafilomycin A1 on lysosomal pH. Cells were treated as in **A**, in the presence or absence of 10 nmol/L bafilomycin A1, and processed as in **B**. **E,** Effect of bafilomycin A1 on the sensitivity of BT474 to T-DM1. Parental BT474 and the T-DM1–resistant clones were treated with 5 nmol/L T-DM1, 1 nmol/L bafilomycin A1, or both for 5 days. Proliferation was measured by MTT metabolization and normalized to control untreated cells. Graph bars represent the mean ± SD of three independent experiments. **F,** Schematic representation of a proposed T-DM1–resistance model. T-DM1 binds HER2 on the plasma membrane, followed by entry of HER2–T-DM1 complexes into the cell via receptor-mediated endocytosis. The internalized complexes are initially contained within endocytic vesicles, which fuse to become early endosomes. The load of these endosomes can be recycled back to the plasma membrane or early endosomes can mature to lysosomes. In the normal pathway, the acidic lysosomal proteases degrade the antibody moiety of the T-DM1, releasing the payload. Intracellular Lys-MCC-DM1 inhibits microtubule polymerization, inducing mitotic arrest, apoptosis, mitotic catastrophe, and disrupted intracellular trafficking. In the resistance pathway, altered lysosomal pH could restrict the intrinsic proteinase activities of lysosomal enzymes impairing proteolytic cleavage of endocytosed T-DM1. The ADC would be retained inside the lysosomes and the payload would not reach its target.

Published OnlineFirst July 7, 2017; DOI: 10.1158/0008-5472.CAN-16-3127

confirmed that lysosomal derangement may lead to T-DM1 inefficacy. Not only this scenario approaches to the clinical setting, but also offers confirmation that such mechanism is not exclusive of BT474 cells made resistant to the drug.

Several important conclusions can be extracted from the studies herewith reported. On one hand, our studies suggest the existence of several mechanisms of resistance to T-DM1 in $HER2^+$ breast cancer cells, one of then linked to deficient lysosomal activity. Such altered lysosomal function may impair processing of T-DM1, limiting its anti-tumoral action. Various experimental data support the existence of diverse mechanisms of T-DM1 resistance, and included (i) genomic analyses, which indicated differences in the DEGs among the T-DM1–resistant clones, (ii) animal studies, which revealed variety in the *in vivo* behavior of tumors in mice injected with cells of the resistant clones, and (iii) cell biological and biochemical data, which showed lysosomal accumulation of T-DM1 and impaired lysosomal function in some of the resistant clones. These interclonal differences demonstrate the existence of multiple mechanisms of resistance to T-DM1, as occurs in the case of other anti-HER2 therapies (45). This could somehow be expected, but is unfortunate from the clinical point of view, as it will imply the knowledge of all the resistance mechanisms to design active anti-tumoral strategies to fight T-DM1 resistance.

Finally, the description of such resistance mechanism may have several important general implications, beyond its identification as a mechanism of T-DM1 resistance. Given the expansion of ADC-based therapeutics, our findings may be relevant to understand resistances raised to other ADCs using the same internalization-degradation pathway for generation of active payloads (46). In addition, our findings suggest the possibility of manipulating the lysosomal pH to augment/restore the anti-tumoral properties of T-DM1 and other ADCs. In this respect, it is interesting to mention a recent report that used photoactivatable nanoparticles to manipulate intralysosomal pH (47). Strategies in that direction could improve ADC-based therapies.

Disclosure of Potential Conflicts of Interest

No potential conflicts of interest were disclosed.

Authors' Contributions

Conception and design: C. Ríos-Luci, S. García-Alonso, E. Díaz-Rodríguez, J. Arribas, A. Ocaña, A. Pandiella

Development of methodology: C. Ríos-Luci, S. García-Alonso, M. Nadal-Serrano, A. Ocaña, A. Pandiella

Acquisition of data (provided animals, acquired and managed patients, provided facilities, etc.): C. Ríos-Luci, S. García-Alonso, E. Díaz-Rodríguez, M. Nadal-Serrano, A. Pandiella

Analysis and interpretation of data (e.g., statistical analysis, biostatistics, computational analysis): C. Ríos-Luci, S. García-Alonso, E. Díaz-Rodríguez, A. Pandiella

Writing, review, and/or revision of the manuscript: C. Ríos-Luci, S. García-Alonso, E. Díaz-Rodríguez, J. Arribas, A. Ocaña, A. Pandiella

Study supervision: C. Ríos-Luci, S. García-Alonso, A. Pandiella

Grant Support

This work was supported by the Ministry of Economy and Competitiveness of Spain (BFU2012-39151 and BFU2015-71371-R), the Instituto de Salud Carlos III through the Spanish Cancer Centers Network Program (RD12/0036/0003), and the Scientific Foundation of the Spanish Association Against Cancer (AECC) and the CRIS Cancer Foundation. S. García-Alonso is recipient of a predoctoral contract from the MINECO (BES-2013-065223). The Cancer Research Institute and the work carried out at our laboratory receive support from the European Community through the Regional Development Funding Program (FEDER). Work in J. Arribas lab was supported with funds from the Instituto de Salud Carlos III (PI16/00253) and the Breast Cancer Research Foundation (BCRF).

The costs of publication of this article were defrayed in part by the payment of page charges. This article must therefore be hereby marked *advertisement* in accordance with 18 U.S.C. Section 1734 solely to indicate this fact.

Received November 16, 2016; revised April 12, 2017; accepted June 29, 2017; published OnlineFirst July 7, 2017.

References

1. Slamon DJ, Clark GM, Wong SG, Levin WJ, Ullrich A, McGuire WL. Human breast cancer: correlation of relapse and survival with amplification of the HER-2/neu oncogene. Science 1987;235:177–82.
2. Di Fiore PP, Pierce JH, Kraus MH, Segatto O, King CR, Aaronson SA. erbB-2 is a potent oncogene when overexpressed in NIH/3T3 cells. Science 1987;237:178–82.
3. Baselga J, Arteaga CL. Critical update and emerging trends in epidermal growth factor receptor targeting in cancer. J Clin Oncol 2005;23:2445–59.
4. Arteaga CL, Engelman JA. ERBB receptors: from oncogene discovery to basic science to mechanism-based cancer therapeutics. Cancer Cell 2014;25:282–303.
5. Moasser MM, Krop IE. The evolving landscape of HER2 targeting in breast cancer. JAMA Oncol 2015;1:1154–61.
6. Carter P, Presta L, Gorman CM, Ridgway JB, Henner D, Wong WL, et al. Humanization of an anti-p185HER2 antibody for human cancer therapy. Proc Natl Acad Sci U S A 1992;89:4285–9.
7. Franklin MC, Carey KD, Vajdos FF, Leahy DJ, de Vos AM, Sliwkowski MX. Insights into ErbB signaling from the structure of the ErbB2-pertuzumab complex. Cancer Cell 2004;5:317–28.
8. Clynes RA, Towers TL, Presta LG, Ravetch JV. Inhibitory Fc receptors modulate in vivo cytotoxicity against tumor targets. Nat Med 2000;6:443–6.
9. Xia W, Mullin RJ, Keith BR, Liu LH, Ma H, Rusnak DW, et al. Anti-tumor activity of GW572016: a dual tyrosine kinase inhibitor blocks EGF activation of EGFR/erbB2 and downstream Erk1/2 and AKT pathways. Oncogene 2002;21:6255–63.
10. Peters C, Brown S. Antibody–drug conjugates as novel anti-cancer chemotherapeutics. Biosci Rep 2015;35:e00225.
11. Lewis Phillips GD, Li G, Dugger DL, Crocker LM, Parsons KL, Mai E, et al. Targeting HER2-positive breast cancer with trastuzumab-DM1, an antibody–cytotoxic drug conjugate. Cancer Res 2008;68:9280–90.
12. Lambert JM, Chari RV. Ado-trastuzumab Emtansine (T-DM1): an antibody–drug conjugate (ADC) for HER2-positive breast cancer. J Med Chem 2014;57:6949–64.
13. Barok M, Tanner M, Koninki K, Isola J. Trastuzumab-DM1 causes tumour growth inhibition by mitotic catastrophe in trastuzumab-resistant breast cancer cells in vivo. Breast Cancer Res 2011;13:R46.
14. Montero JC, Garcia-Alonso S, Ocana A, Pandiella A. Identification of therapeutic targets in ovarian cancer through active tyrosine kinase profiling. Oncotarget 2015;6:30057–71.
15. Amiri-Kordestani L, Blumenthal GM, Xu QC, Zhang L, Tang SW, Ha L, et al. FDA approval: ado-trastuzumab emtansine for the treatment of patients with HER2-positive metastatic breast cancer. Clin Cancer Res 2014;20:4436–41.
16. Verma S, Miles D, Gianni L, Krop IE, Welslau M, Baselga J, et al. Trastuzumab emtansine for HER2-positive advanced breast cancer. N Engl J Med 2012;367:1783–91.
17. Krop IE, Kim SB, Gonzalez-Martin A, LoRusso PM, Ferrero JM, Smitt M, et al. Trastuzumab emtansine versus treatment of physician's choice for pretreated HER2-positive advanced breast cancer (TH3RESA): a randomised, open-label, phase 3 trial. Lancet Oncol 2014;15:689–99.

18. Montero JC, Chen X, Ocana A, Pandiella A. Predominance of mTORC1 over mTORC2 in the regulation of proliferation of ovarian cancer cells: therapeutic implications. Mol Cancer Ther 2012;11:1342–52.
19. Vicario R, Peg V, Morancho B, Zacarias-Fluck M, Zhang J, Martinez-Barriocanal A, et al. Patterns of HER2 gene amplification and response to anti-HER2 therapies. PLoS One 2015;10:e0129876.
20. Borges J, Pandiella A, Esparis-Ogando A. Erk5 nuclear location is independent on dual phosphorylation, and favours resistance to TRAIL-induced apoptosis. Cell Signal 2007;19:1473–87.
21. Seoane S, Montero JC, Ocana A, Pandiella A. Breast cancer dissemination promoted by a neuregulin-collagenase 3 signalling node. Oncogene 2016;35:2756–65.
22. Chen EY, Tan CM, Kou Y, Duan Q, Wang Z, Meirelles GV, et al. Enrichr: interactive and collaborative HTML5 gene list enrichment analysis tool. BMC Bioinformatics 2013;14:128.
23. Kuleshov MV, Jones MR, Rouillard AD, Fernandez NF, Duan Q, Wang Z, et al. Enrichr: a comprehensive gene set enrichment analysis web server 2016 update. Nucleic Acids Res 2016;44(W1):W90–7.
24. Cabrera N, Diaz-Rodriguez E, Becker E, Martin-Zanca D, Pandiella A. TrkA receptor ectodomain cleavage generates a tyrosine-phosphorylated cell-associated fragment. J Cell Biol 1996;132:427–36.
25. Yuste L, Montero JC, Esparis-Ogando A, Pandiella A. Activation of ErbB2 by overexpression or by transmembrane neuregulin results in differential signaling and sensitivity to herceptin. Cancer Res 2005;65:6801–10.
26. Diaz-Rodriguez E, Alvarez-Fernandez S, Chen X, Paiva B, Lopez-Perez R, Garcia-Hernandez JL, et al. Deficient spindle assembly checkpoint in multiple myeloma. PLoS One 2011;6:e27583.
27. Montero JC, Esparis-Ogando A, Re-Louhau MF, Seoane S, Abad M, Calero R, et al. Active kinase profiling, genetic and pharmacological data define mTOR as an important common target in triple-negative breast cancer. Oncogene 2014;33:148–56.
28. Barok M, Joensuu H, Isola J. Trastuzumab emtansine: mechanisms of action and drug resistance. Breast Cancer Res 2014;16:209.
29. Arribas J, Baselga J, Pedersen K, Parra-Palau JL. p95HER2 and breast cancer. Cancer Res 2011;71:1515–9.
30. Niikura N, Liu J, Hayashi N, Mittendorf EA, Gong Y, Palla SL, et al. Loss of human epidermal growth factor receptor 2 (HER2) expression in metastatic sites of HER2-overexpressing primary breast tumors. J Clin Oncol 2012;30:593–9.
31. Moasser MM. Targeting the function of the HER2 oncogene in human cancer therapeutics. Oncogene 2007;26:6577–92.
32. Nagata Y, Lan KH, Zhou X, Tan M, Esteva FJ, Sahin AA, et al. PTEN activation contributes to tumor inhibition by trastuzumab, and loss of PTEN predicts trastuzumab resistance in patients. Cancer Cell 2004;6:117–27.
33. Eichhorn PJ, Gili M, Scaltriti M, Serra V, Guzman M, Nijkamp W, et al. Phosphatidylinositol 3-kinase hyperactivation results in lapatinib resistance that is reversed by the mTOR/phosphatidylinositol 3-kinase inhibitor NVP-BEZ235. Cancer Res 2008;68:9221–30.
34. Hamblett KJ, Jacob AP, Gurgel JL, Tometsko ME, Rock BM, Patel SK, et al. SLC46A3 is required to transport catabolites of noncleavable antibody maytansine conjugates from the lysosome to the cytoplasm. Cancer Res 2015;75:5329–40.
35. El-Sayed A, Futaki S, Harashima H. Delivery of macromolecules using arginine-rich cell-penetrating peptides: ways to overcome endosomal entrapment. AAPS J 2009;11:13–22.
36. Nath N, Godat B, Zimprich C, Dwight SJ, Corona C, McDougall M, et al. Homogeneous plate based antibody internalization assay using pH sensor fluorescent dye. J Immunol Methods 2016;431:11–21.
37. Chan YK, Sung HK, Jahng JW, Kim GH, Han M, Sweeney G. Lipocalin-2 inhibits autophagy and induces insulin resistance in H9c2 cells. Mol Cell Endocrinol 2016;430:68–76.
38. Rodriguez-Arribas M, Yakhine-Diop SM, Gonzalez-Polo RA, Niso-Santano M, Fuentes JM. Turnover of lipidated LC3 and autophagic cargoes in mammalian cells. Methods Enzymol 2017;587:55–70.
39. Klionsky DJ, Abdelmohsen K, Abe A, Abedin MJ, Abeliovich H, Acevedo Arozena A, et al. Guidelines for the use and interpretation of assays for monitoring autophagy (3rd edition). Autophagy 2016;12:1–222.
40. Arena S, Bellosillo B, Siravegna G, Martinez A, Canadas I, Lazzari L, et al. Emergence of multiple EGFR extracellular mutations during cetuximab treatment in colorectal cancer. Clin Cancer Res 2015;21:2157–66.
41. Junttila TT, Li G, Parsons K, Phillips GL, Sliwkowski MX. Trastuzumab-DM1 (T-DM1) retains all the mechanisms of action of trastuzumab and efficiently inhibits growth of lapatinib insensitive breast cancer. Breast Cancer Res Treat 2011;128:347–56.
42. Kovtun YV, Goldmacher VS. Cell killing by antibody–drug conjugates. Cancer Lett 2007;255:232–40.
43. Sorkin A, Goh LK. Endocytosis and intracellular trafficking of ErbBs. Exp Cell Res 2008;314:3093–106.
44. Baulida J, Kraus MH, Alimandi M, Di Fiore PP, Carpenter G. All ErbB receptors other than the epidermal growth factor receptor are endocytosis impaired. J Biol Chem 1996;271:5251–7.
45. Gagliato DM, Jardim DL, Marchesi MS, Hortobagyi GN. Mechanisms of resistance and sensitivity to anti-HER2 therapies in HER2^{+} breast cancer. Oncotarget 2016;7:64431–46.
46. Erickson HK, Park PU, Widdison WC, Kovtun YV, Garrett LM, Hoffman K, et al. Antibody–maytansinoid conjugates are activated in targeted cancer cells by lysosomal degradation and linker-dependent intracellular processing. Cancer Res 2006;66:4426–33.
47. Trudeau KM, Colby AH, Zeng J, Las G, Feng JH, Grinstaff MW, et al. Lysosome acidification by photoactivated nanoparticles restores autophagy under lipotoxicity. J Cell Biol 2016;214:25–34.

Published OnlineFirst July 7, 2017; DOI: 10.1158/0008-5472.CAN-16-3127

Cancer Research
The Journal of Cancer Research (1916–1930) | The American Journal of Cancer (1931–1940)

AACR American Association for Cancer Research

Resistance to the Antibody–Drug Conjugate T-DM1 Is Based in a Reduction in Lysosomal Proteolytic Activity

Carla Ríos-Luci, Sara García-Alonso, Elena Díaz-Rodríguez, et al.

Cancer Res 2017;77:4639-4651. Published OnlineFirst July 7, 2017.